A comprehensive study of *RXTE* and *INTEGRAL* observations of the X-ray pulsar 4U 1907+09

Ş. Şahiner,[1][*] S. Ç. İnam[2][*] and A. Baykal[1][*]

[1]*Physics Department, Middle East Technical University, 06531 Ankara, Turkey*
[2]*Department of Electrical and Electronics Engineering, Başkent University, 06530 Ankara, Turkey*

ABSTRACT

We analyse observations of the accretion-powered pulsar 4U 1907+09 from the *International Gamma-Ray Astrophysics Laboratory* (*INTEGRAL*; between 2005 October and 2007 November) and from the *Rossi X-ray Timing Explorer* (*RXTE*; between 2007 June and 2011 March). Using observations from the Imager on-board the *INTEGRAL* satellite (IBIS), the *INTEGRAL* Soft Gamma-Ray Imager (ISGRI) and the *RXTE* Proportional Counter Array (PCA), we update the pulse period history of the source. We construct power spectrum density of pulse frequencies, and we find that fluctuations in the pulse frequency derivatives are consistent with the random walk model with a noise strength of 1.27×10^{-21} Hz s^{-2}. From the X-ray spectral analysis of *RXTE*/PCA observations, we find that the hydrogen column density is variable over the binary orbit, and that it tends to increase just after the periastron passage. We also show that the X-ray spectrum becomes hardened with decreasing X-ray flux. We discuss the pulse-to-pulse variability of the source near dipping ingress and egress. We find that the source is more likely to undergo dipping states after apastron until periastron when the accretion from clumpy wind might dominate. Thus, occasional transitions to a temporary propeller state might occur.

Key words: accretion, accretion discs – stars: neutron – pulsars: individual: 4U 1907+09 – X-rays: binaries.

1 INTRODUCTION

The X-ray source 4U 1907+09 was discovered in the early 1970s by the *Uhuru* survey (Giacconi et al. 1971). The system is a high-mass X-ray binary (HMXB), which contains an X-ray pulsar accreting material from its blue supergiant companion star. The pulsar has an eccentric ($e \sim 0.28$) orbit around its companion, and the orbital period of the binary system is $\sim$8.3753 d (In't Zand, Baykal & Strohmayer 1998).

The orbital profile of 4U 1907+09 exhibits two flares per orbit, separated by a $\simeq$0.5 orbital phase: a large primary at the periastron and a small secondary at the apastron (Marshall & Ricketts 1980; In't Zand et al. 1998). The presence of the two phase-locked flares has led to the suggestion that the compact object passes through a circumstellar disc of matter around the equatorial plane of a Be-type stellar companion (Iye 1986; Cook & Page 1987). However, the position of 4U 1907+09 in the Corbet diagram (Corbet 1984) indicates that the companion is probably an OB-type supergiant. The latest optical (Cox, Kaper & Mokiem 2005) and infrared (Nespoli, Fabregat & Mennickent 2008) observations have actually shown

that the companion could be classified as an O8–O9 Ia supergiant, with a mass-loss rate of $\dot{M} = 7 \times 10^{-6}$ M$_\odot$ yr^{-1} and a lower limit of distance of $\sim$5 kpc.

The spin period of 4U 1907+09 was first measured as $\sim$437.5 s using *Tenma* observations (Makishima et al. 1984). The pulse profile is known to be double-peaked with variable amplitude. The profile is insensitive to energies below 20 keV, whereas dramatic changes are present above 20 keV (In't Zand et al. 1998). Historical period measurements confirm that the pulsar has been steadily spinning down since its discovery until 1998, with an average rate of $\dot{\nu} = -3.54 \times 10^{-14}$ Hz s^{-1} (Cook & Page 1987; In't Zand et al. 1998; Baykal et al. 2001; Mukerjee et al. 2001). In 2001, *Rossi X-ray Timing Explorer* (*RXTE*) observations showed that the spin rate was lowered by a factor of $\sim$0.60 (Baykal, İnam & Beklen 2006). From *International Gamma-Ray Astrophysics Laboratory* (*INTEGRAL*) observations, it was reported that the spin period had reached a maximum of $\sim$441.3 s, after which a torque reversal occurred and the source began to spin up with a rate of 2.58×10^{-14} Hz s^{-1} after 2004 May (Fritz et al. 2006). Recent measurements with *RXTE*, which are presented in İnam, Şahiner & Baykal (2009a) and this paper, have revealed that 4U 1907+09 has returned to a spin-down trend with a rate of -3.59×10^{-14} Hz s^{-1}, which is close to the previous steady spin-down rate. This implies that another torque reversal could have taken place before 2007 June.

[*]E-mail: seyda@astroa.physics.metu.edu.tr (ŞŞ); inam@baskent.edu.tr (SÇİ); altan@astroa.physics.metu.edu.tr (AB)

4U 1907+09 has been identified as a variable X-ray source, showing irregular flaring and dipping activities, and for ∼20 per cent of its observations, it has been reported to be in a dip state with no detectable pulsed emission (In't Zand, Strohmayer & Baykal 1997). The typical duration of the dips has been found to vary between a few minutes and 1.5 h. Variations in the X-ray flux are accepted as evidence of instability in the mass accretion rate, where dipping states are associated with the cessation of accretion from the inhomogeneous wind of the companion star.

The X-ray spectra of 4U 1907+09 have basically been described by a power law with a photon index ∼1.2 and an exponential cut-off at ∼13 keV (Schwartz et al. 1980; Marshall & Ricketts 1980; Makishima et al. 1984; Cook & Page 1987; Chitnis et al. 1993; Roberts et al. 2001; Coburn et al. 2002; Baykal et al. 2006; Fritz et al. 2006). The continuum was found to be modified by a highly variable hydrogen column density (n_H) over the binary orbit, between 1×10^{22} and 9×10^{22} cm^{-2}, as a consequence of inhomogeneous accretion via dense stellar wind (In't Zand et al. 1997). A narrow spectral line around 6.4 keV, corresponding to the Fe Kα emission produced by the fluorescence of matter surrounding the pulsar, was also observed in the spectra. A detailed determination of the Fe K emission complex has recently been reported using *Suzaku* observations, wherein Fe Kβ emission has been detected for the first time (Rivers et al. 2010). Observations with *Ginga* (Mihara 1995; Makishima et al. 1999) and *BeppoSAX* (Cusumano et al. 1998) have exhibited cyclotron resonant scattering features (CRSFs) at higher energies. The line energies of the fundamental and second harmonic cyclotron lines were found to be ∼19 and ∼39 keV, respectively, implying a surface magnetic field strength of 2.1 × 10^{12} G (Cusumano et al. 1998).

In this paper, we present a timing and spectral analysis of the *RXTE* monitoring observations of 4U 1907+09 between 2007 June and 2011 March. Selected *INTEGRAL* pointing observations are analysed to cover the gap in the spin-period history. We describe the observations in Section 2, and we report on the pulse timing analysis in Section 3. In Section 4, we discuss the spectral results, and in Section 5, we focus on the dipping states of the source. Finally, we summarize our results in Section 6.

2 OBSERVATIONS

2.1 *RXTE*

One of the main instruments on-board *RXTE* is the Proportional Counter Array (PCA), which consists of five co-aligned identical proportional counter units (PCUs) pointed at the same location in the sky (Jahoda et al. 1996). The field of view (FOV) of the PCA at full width at half-maximum (FWHM) is about 1° and the effective area of each detector is approximately 1300 cm^2. The PCA operates in the energy range 2–60 keV, with an energy resolution of 18 per cent at 6 keV.

In this paper, we present a timing and spectral analysis of 98 pointed *RXTE*/PCA observations of 4U 1907+09 between 2007 June and 2011 March, each with an exposure of ∼2 ks (see Table 1). A preliminary timing analysis has already been performed and the corresponding spin-rate measurements have been presented previously by İnam et al. (2009a) and Şahiner, İnam & Baykal (2011). In this paper, we extend this analysis by using observations with a longer time-span, by performing a more detailed timing analysis and by presenting the results of our spectral analysis.

Although the number of active PCUs during the observations of 4U 1907+09 varies between one and three, the data obtained from

Table 1. Log of the *RXTE* observations of 4U 1907+09.

RXTE proposal ID	Time (MJD)	Number of observations	Exposure (ks)
93036	54280–54825	39	74.1[a,b]
94036	54839–55184	24	45.3[b]
95350	55208–55555	26	49.4
96366	55571–55638	9	47.2

[a]The results from the first 30 observations have been published previously by İnam et al. (2009a).
[b]The preliminary timing analysis results have been presented previously by Şahiner et al. (2011).

PCUs 0 and 1 are not appropriate for spectral analysis because of the increased background levels as a result of the loss of their propane layers. Consequently, the only data products taken into consideration during the spectral analysis belong to PCU 2, in order to avoid probable problems because of calibration differences between the detectors. The loss of the propane layers of PCU 0 and PCU 1 does not affect the high-resolution timing, and therefore no PCU selection is done for the timing analysis.

The standard software tools of HEASOFT v.6.10 are used for the analysis of the PCA data. Filter files are produced to apply constraints on the data such that the times when the elevation angle is less than 10°, when the offset from the source is greater than 0.02° and when the electron contamination of PCU 2 is greater than 0.1 are excluded. The data modes examined for the spectral and light-curve extraction are the Standard2f and GoodXenon modes, respectively. The background spectra and light curves are generated by the latest PCA background estimator models supplied by the *RXTE* Guest Observer Facility (GOF), EPOCH 5C.

2.2 *INTEGRAL*

The *INTEGRAL* observations analysed in this paper are obtained from the archive of the *INTEGRAL* Science Data Centre (ISDC). All publicly available pointing observations subsequent to the previous study of 4U 1907+09 (Fritz et al. 2006) are selected, considering the good times from the Imager on-board the *INTEGRAL* Satellite–*INTEGRAL* Soft Gamma-Ray Imager (IBIS–ISGRI) to be above 1 ks. Selected observations, in which the source is in the FOV with an offset angle smaller than 5°, are taken to be between 2005 October and 2007 November. The data consist of a total of 611 science windows (SCWs; each ∼3 ks) within revolutions 366 and 623.

The data products of the IBIS–ISGRI detector on-board *INTEGRAL* are reduced for the analysis. IBIS is a coded mask instrument, which has a fully coded FOV of 8°.3 × 8°.0 and 12-arcmin angular resolution (FWHM; Ubertini et al. 2003). ISGRI is the upper layer of the IBIS instrument, which operates in the energy range between 15 keV and 1 MeV, with an energy resolution of 8 per cent at 60 keV (Lebrun et al. 2003). The data reduction is performed by the software OSA v.7.0. The standard pipeline processing comprises gain correction, good-time handling, dead-time derivation, background correction and energy reconstruction. Images in two energy bands (20–40 and 40–60 keV) are produced from IBIS–ISGRI data with the use of an input catalogue consisting of strong sources in the FOV: Ser X-1, XTE J1855−026, 4U 1909+07, SS 433, IGR J19140+0951, GRS 1915+105 and 4U 1907+09. The background maps provided by the ISGRI team are used for background correction. Light curves are created by the tool II_LIGHT, which allows high-resolution timing.
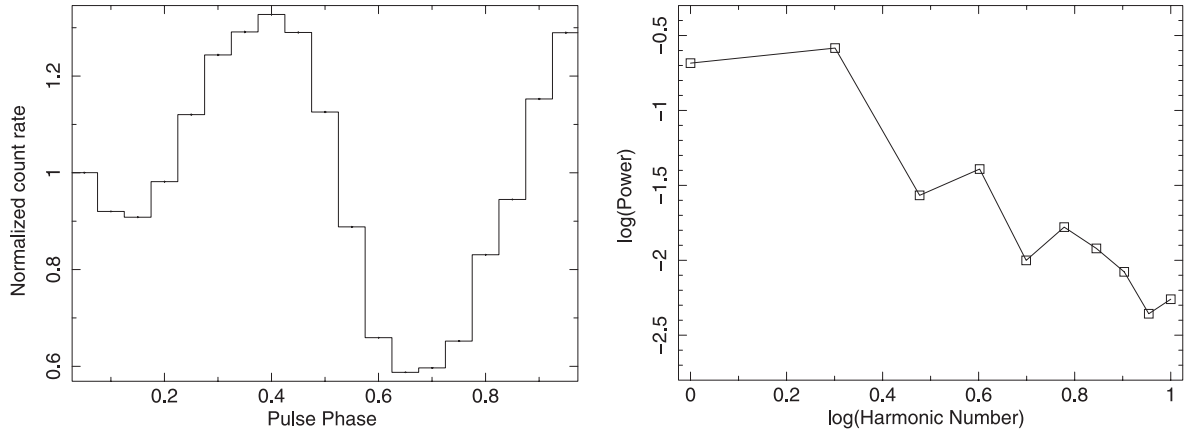
Figure 1. A sample template pulse profile (left) and its power spectra (right) in terms of harmonic number obtained from the observation of MJD 55586.

3 TIMING ANALYSIS

3.1 Pulse frequency measurements

For timing analysis, we use 1-s binned background-corrected *RXTE*/PCA light curves of the source. These background-subtracted light curves are corrected to the barycentre of the Solar system. Then, we correct the light curves for the binary motion of 4U 1907+09 using the binary orbital parameters (In't Zand et al. 1998). Because 4U 1907+09 has many dips, we eliminate these dips from the light curve. Pulse periods for 4U 1907+09 are found by folding the time series on statistically independent trial periods (Leahy et al. 1983). Template pulse profiles are constructed from these observations by folding the data on the period giving maximum χ^2. The pulse profiles consist of 20 phase bins and are represented by their Fourier harmonics (Deeter & Boynton 1985). We present a sample template pulse profile and its power spectra in terms of harmonic number in Fig. 1.

The pulse arrival times are obtained from the cross-correlation between the template and pulse profiles obtained in each ∼2-ks observation. We have been able to connect all pulse arrival times of the *RXTE* observations in phase over a 1300-d time-span. In the phase connection procedure, in order to avoid cycle count ambiguity, we construct the pulse arrival times for a time-span where the maximum phase shift is less than 1. This time-scale for 4U 1907+09 is around 160 d. We divide the total time-span into 10 time intervals, each around 160 d, and we construct the pulse arrival times with respect to the best period in that time interval. Then, we align the slopes of the pulse arrival times in the overlapping time intervals and we construct pulse arrival times, as presented in the upper panel of Fig. 2.

We fit the pulse arrival times to the fifth-order polynomial:

$$\delta\phi = \delta\phi_0 + \delta\nu(t - t_0) + \sum_{n=2}^{5} \frac{1}{n!} \frac{d^n\phi}{dt^n} (t - t_0)^n. \quad (1)$$

Here, $\delta\phi$ is the pulse phase offset deduced from the pulse timing analysis, t_0 is the mid-time, $\delta\phi_0$ is the residual phase offset at t_0, $\delta\nu$ is the correction to the pulse frequency at time t_0, and $d^n\phi/dt^n$ for $n = 2, 3, 4$ and 5 are the first-, second-, third- and fourth-order derivatives of the pulse phase, respectively.

Fig. 2 presents the pulse arrival times (pulse cycles) and the residuals of the fit after the removal of the fifth-order polynomial trend. Table 2 presents the timing solution of 4U 1907+09 between MJD 54280 and 55600. It should be noted that we have also obtained
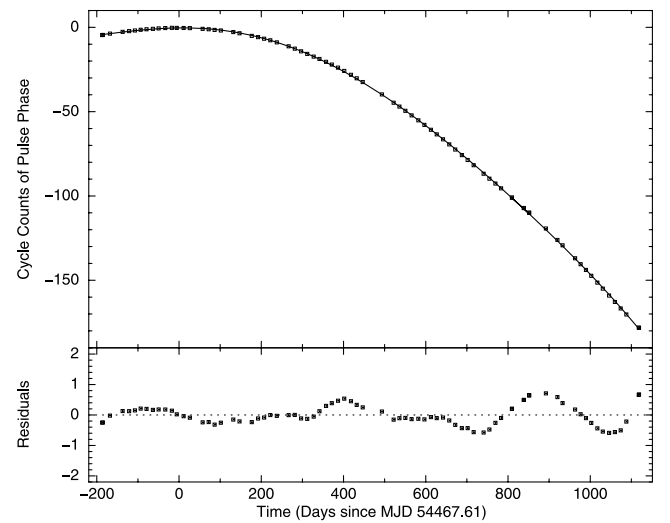

Figure 2. Cycle counts of pulse phase and the best-fitting model (solid line). The residuals after the removal of the fifth-order polynomial (see equation 1) are given in the bottom panel.

Table 2. Pulse timing solution of 4U 1907+09 between MJD 54280 and 55600.

Parameter	Value
Epoch (t_0)	MJD 54467.61(6)
Pulse period (P)	441.2088(2) s
Spin frequency (ν)	$2.2665002(8) \times 10^{-3}$ Hz
$\dot{\nu}$	$-3.672(1) \times 10^{-14}$ Hz s^{-1}
$\ddot{\nu}$	$-1.497(5) \times 10^{-21}$ Hz s^{-2}
$\dddot{\nu}$	$1.063(9) \times 10^{-28}$ Hz s^{-3}
$\ddddot{\nu}$	$-2.44(3) \times 10^{-36}$ Hz s^{-4}
RMS residual (pulse phase)	0.32

pulse residuals by performing pulse timing analysis using the timing solution parameters for the pulse frequency and its time derivatives given in Table 2.

In order to obtain pulse frequencies, we fit a linear model to each successive pair of arrival times. The slopes of these linear fits lead us to estimate the pulse frequency values at the mid-time of the corresponding observations. In Fig. 3 and Table 3, we present the pulse period history of the source. In order to check the reliability of pulse arrival times, we also obtained the pulse periods using the
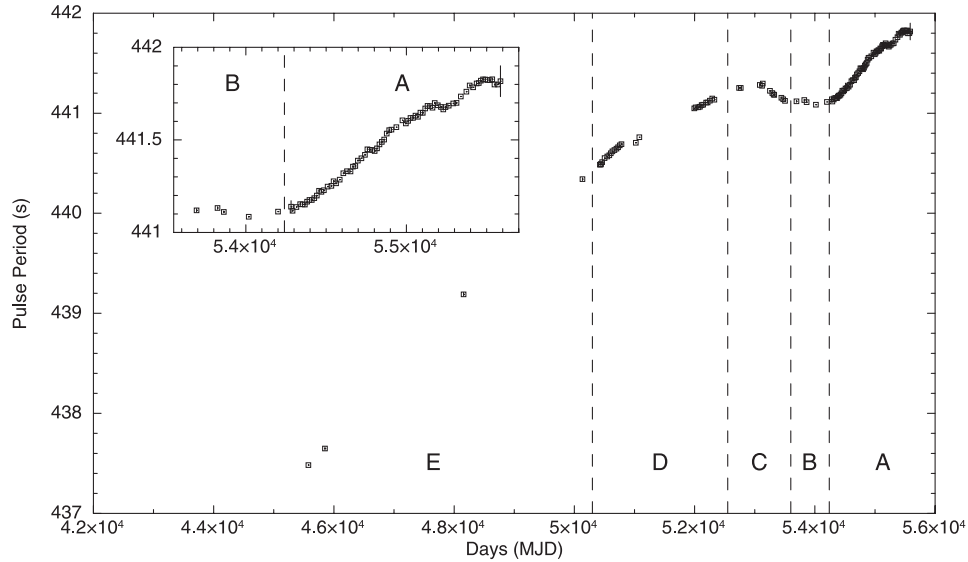
© 2012 The Authors, MNRAS **421**, 2079–2087
Monthly Notices of the Royal Astronomical Society © 2012 RAS

Figure 3. Pulse period history of 4U 1907+09. The measurements from *RXTE* and *INTEGRAL* used in this paper and in İnam et al. (2009a) lie in regions A and B, respectively. They are plotted separately in the inset (see Table 3). Measurements from Fritz et al. (2006) and Baykal et al. (2001, 2006) are in regions C and D, respectively. The oldest measurements lie in region E (Makishima et al. 1984; Cook & Page 1987; Mihara 1995; In't Zand et al. 1998).

slopes of pulse arrivals times obtained from 160-d time intervals. We found exactly the same pulse periods as obtained from the arrival times of the 1300-d time-span. Using the pulse periods, we obtained the pulse frequency value of $\dot{\nu} = -3.672(1) \times 10^{-14}$ Hz s^{-1} for a time-span of ~1300 d. This is also consistent with the timing solution in Table 2.

For the timing analysis of the *INTEGRAL* observations, we extract 10-s binned background-corrected IBIS–ISGRI light curves in the energy range 20–40 keV. We sample light curves from the ~7–10-d time-span and we find the best pulse frequency by folding the light curve on statistically independent pulse frequencies. Then, by constructing master and sample pulse profiles, we obtain pulse arrival times as described above. From the slopes of the pulse arrival times ($\delta\phi = \delta\nu(t - t_0)$), we attain the correction for pulse frequencies. We present pulse frequencies measured from *RXTE*/PCA and *INTEGRAL* IBIS–ISGRI observations in Fig. 3 and Table 3.

3.2 Torque noise strength

In order to see the statistical trend of the pulse frequency derivatives, we construct a power spectrum of the pulse frequency derivatives. We use the Deeter polynomial estimator method (Deeter 1984) for the pulse frequency measurements. This technique uses polynomial estimators instead of sinusoidal estimates for each time-scale T.

The power density spectra can be expressed by applying a sampling function to the pulse arrival times (Deeter 1984; for the applications, see Bildsten et al. 1997; Baykal et al. 2007). The power density estimator $P_{\dot{\nu}}(f)$ is defined as $\int_0^\infty P_{\dot{\nu}}(f)\,\mathrm{d}f = \langle(\dot{\nu} - \langle\dot{\nu}\rangle)^2\rangle$, where $\langle\dot{\nu}\rangle$ is the mean pulse frequency derivative for a given analysis frequency. In order to estimate the power density, we first divide pulse arrival times into time-spans of duration T and we fit the cubic polynomial in time. The observed time series is simulated by Monte Carlo techniques, for a unit white noise strength defined as $P_{\dot{\nu}}(f) = 1$, and it is fitted to a cubic polynomial in time. Then, the square of the third-order polynomial term is divided into the value from the Monte Carlo simulations (Cordes 1980; Deeter 1984). The logarithmic average of these estimators over the same time intervals is the power density estimate. This procedure is repeated for

different durations T to obtain a power spectrum. We have also calculated the power density with the quartic polynomial estimator, and we have found that the power density spectra are consistent with the cubic polynomial estimator. The frequency responses of each power density and the measurement noise estimates are presented at $f \sim 1/T$. In Fig. 4, we present the power of the pulse frequency derivatives, $P_{\dot{\nu}}(f)$, per Hertz as a function of analysis frequency f. The slope of the power spectrum between 1/1300 and 1/75 d^{-1} is flat. This suggests that fluctuations in the pulse frequency derivatives are white noise and the pulse frequency fluctuations are consistent with the random walk model. The noise strength is found to be 1.27×10^{-21} Hz s^{-2}.

The random walk model in the pulse frequency or the white noise model in pulse frequency derivative are appropriate models for wind accretors (e.g. Vela X-1, 4U 1538-52 and GX 301-2; Deeter 1981; Deeter et al. 1989; Bildsten et al. 1997). They have flat power spectra with white noise strength in the range 10^{-20}–10^{-18} Hz s^{-2}. However, Her X-1 and 4U 1626-67 are disc accretors with low-mass companions, which have shown pulse frequency time series consistent with the random walk model (Bildsten et al. 1997). Their white noise strengths are in the range 10^{-21} to 10^{-18} Hz s^{-2}. In these systems, red noise in the pulse frequency cannot be ruled out (Bildsten et al. 1997). For disc accretors, Cen X-3 has red noise in the pulse frequency derivatives, and the noise strength varies from low to high frequencies such as 10^{-16} and 10^{-18} Hz s^{-2} (Bildsten et al. 1997). The power-law index of the power spectra in this system is ~ -1. This implies that, at short time-scales, disc accretion is dominant and the noise is less; however, at time-scales longer than viscous time-scales, there is excessive noise.

4 SPECTRAL ANALYSIS

4.1 Orbital phase-resolved spectra with *RXTE*/PCA

The *RXTE* observations of 4U 1907+09 were proposed with a time distribution such that they spread over a variety of orbital phases. Therefore, these observations are very suitable for investigating the variation in the spectral parameters through the binary orbit. During

Table 3. Pulse period measurements of 4U 1907+09.

Epoch (MJD)	Pulse period (s)	Reference	Epoch (MJD)	Pulse period (s)	Reference
53693.0	441.1193 ± 0.0100	This work[a]	54877.5	441.5344 ± 0.0035	This work[b]
53823.6	441.1322 ± 0.0070	This work[a]	54892.7	441.5526 ± 0.0040	This work[b]
53862.6	441.1108 ± 0.0050	This work[a]	54907.0	441.5553 ± 0.0039	This work[b]
54018.1	441.0847 ± 0.0020	This work[a]	54937.6	441.5687 ± 0.0012	This work[b]
54200.4	441.1127 ± 0.0014	This work[a]	54975.3	441.6058 ± 0.0020	This work[b]
54281.5	441.1030 ± 0.0372	İnam et al. (2009a)	54996.5	441.5892 ± 0.0040	This work[b]
54291.0	441.1213 ± 0.0038	İnam et al. (2009a)	55010.7	441.6029 ± 0.0039	This work[b]
54315.0	441.1367 ± 0.0021	İnam et al. (2009a)	55025.6	441.6185 ± 0.0037	This work[b]
54338.2	441.1545 ± 0.0041	İnam et al. (2009a)	55041.4	441.6188 ± 0.0034	This work[b]
54353.3	441.1509 ± 0.0046	İnam et al. (2009a)	55057.0	441.6310 ± 0.0038	This work[b]
54367.3	441.1543 ± 0.0047	İnam et al. (2009a)	55072.3	441.6247 ± 0.0036	This work[b]
54381.3	441.1623 ± 0.0046	İnam et al. (2009a)	55087.2	441.6473 ± 0.0040	This work[b]
54396.2	441.1750 ± 0.0042	İnam et al. (2009a)	55102.0	441.6462 ± 0.0037	This work[b]
54410.9	441.1761 ± 0.0047	İnam et al. (2009a)	55117.2	441.6697 ± 0.0037	This work[b]
54426.0	441.1862 ± 0.0041	İnam et al. (2009a)	55132.0	441.6836 ± 0.0038	This work[b]
54442.1	441.1992 ± 0.0040	İnam et al. (2009a)	55147.4	441.6826 ± 0.0035	This work[b]
54456.1	441.2245 ± 0.0056	İnam et al. (2009a)	55162.5	441.6737 ± 0.0040	This work[b]
54470.4	441.2185 ± 0.0039	İnam et al. (2009a)	55176.8	441.6996 ± 0.0039	This work[b]
54486.3	441.2284 ± 0.0043	İnam et al. (2009a)	55196.2	441.6874 ± 0.0023	This work
54509.4	441.2472 ± 0.0021	İnam et al. (2009a)	55215.3	441.6777 ± 0.0040	This work
54532.3	441.2537 ± 0.0044	İnam et al. (2009a)	55229.7	441.6647 ± 0.0039	This work
54546.8	441.2756 ± 0.0046	İnam et al. (2009a)	55243.9	441.6772 ± 0.0041	This work
54561.6	441.2657 ± 0.0043	İnam et al. (2009a)	55264.0	441.6848 ± 0.0021	This work
54584.3	441.2855 ± 0.0022	İnam et al. (2009a)	55291.7	441.6973 ± 0.0020	This work
54607.1	441.3195 ± 0.0043	İnam et al. (2009a)	55312.5	441.6998 ± 0.0043	This work
54629.6	441.3301 ± 0.0022	İnam et al. (2009a)	55339.4	441.7343 ± 0.0014	This work
54652.1	441.3307 ± 0.0043	İnam et al. (2009a)	55373.8	441.7607 ± 0.0020	This work
54667.2	441.3549 ± 0.0044	İnam et al. (2009a)	55394.1	441.7943 ± 0.0045	This work
54682.1	441.3596 ± 0.0044	İnam et al. (2009a)	55415.6	441.7842 ± 0.0018	This work
54697.5	441.3883 ± 0.0035	This work[b]	55437.5	441.8052 ± 0.0042	This work
54719.7	441.4009 ± 0.0020	This work[b]	55450.7	441.8073 ± 0.0043	This work
54741.6	441.4195 ± 0.0037	This work[b]	55463.7	441.8199 ± 0.0043	This work
54756.8	441.4492 ± 0.0037	This work[b]	55477.6	441.8271 ± 0.0038	This work
54771.9	441.4465 ± 0.0038	This work[b]	55491.5	441.8263 ± 0.0043	This work
54787.2	441.4460 ± 0.0036	This work[b]	55505.8	441.8235 ± 0.0037	This work
54802.1	441.4398 ± 0.0040	This work[b]	55520.5	441.8227 ± 0.0040	This work
54817.2	441.4544 ± 0.0035	This work[b]	55534.6	441.8278 ± 0.0040	This work
54832.1	441.4758 ± 0.0041	This work[b]	55548.6	441.7993 ± 0.0041	This work
54846.6	441.4889 ± 0.0037	This work[b]	55570.5	441.7994 ± 0.0019	This work
54861.8	441.5019 ± 0.0037	This work[b]	55585.8	441.8172 ± 0.0834	This work

[a]The pulse periods are measured from *INTEGRAL* observations.
[b]The pulse periods have been presented previously by Şahiner et al. (2011).

the analysis of the PCA spectra, the energy range is restricted to 3–25 keV because the count statistics is poor beyond this range. The spectral analysis is carried out using the XSPEC v.12.6.0 software. A systematic error of 2 per cent is applied to handle the uncertainties in the response matrices and in the background modelling (Wilms et al. 1999).

4U 1907+09 is near the Galactic plane and the supernova remnant W49B, and therefore an extra process is needed for a correct estimation of the background spectra. The exceptional dipping states of the source provide a good basis for background estimation because the count rates are consistent with the Galactic ridge emission (Roberts et al. 2001; Baykal et al. 2006). 4U 1907+09 is detected to be in the dipping state in about 55 ks of the 216 ks *RXTE*/PCA observations. The overall dipping-state spectrum is used as an additional background; this procedure has previously been explained by İnam et al. (2009a).

A total of 71 non-dip spectra of 4U 1907+09 are analysed for the orbital variation of the spectral parameters. The results of first 19 spectra have also been given in a previous paper (İnam et al. 2009a). The basic model, which consists of a power law (`powerlaw`) with a high-energy cut-off (`highecut`) and photoelectric absorption (`wabs`), is successful for only 10 spectra, so an additional model component for the CRSF around 19 keV is required for the rest. We use the `cyclabs` model in XSPEC (Makishima et al. 1990; Mihara et al. 1990). The fundamental line energy is fixed at 18.9 keV because of the statistical insignificance of the individual PCA spectra with a short exposure time (∼2 ks). The mean values of the depth and the width of the line are found to be 0.4 and 1.7 keV, respectively. These values are used to model the CRSF because they agree within 1σ uncertainty with the previous CRSF parameters (Mihara 1995; Cusumano et al. 1998; Makishima et al. 1999). The addition of a model component for the weak Fe emission line at 6.4 keV did
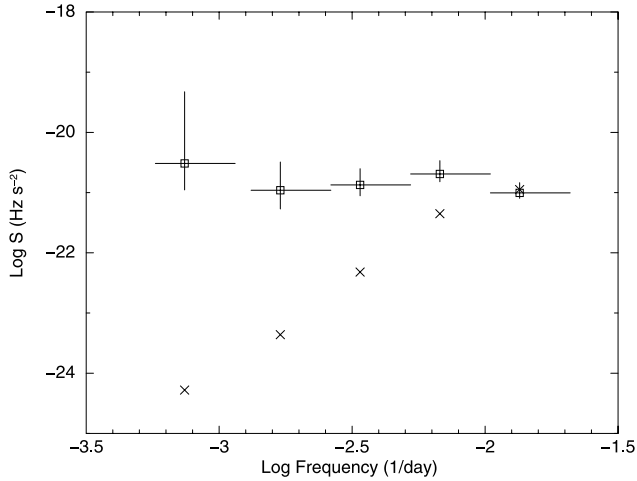
Figure 4. Power density of spin frequency derivatives of 4U 1907+09. The power resulting from measurement noise is subtracted from the estimates, and this is shown independently by the crosses.
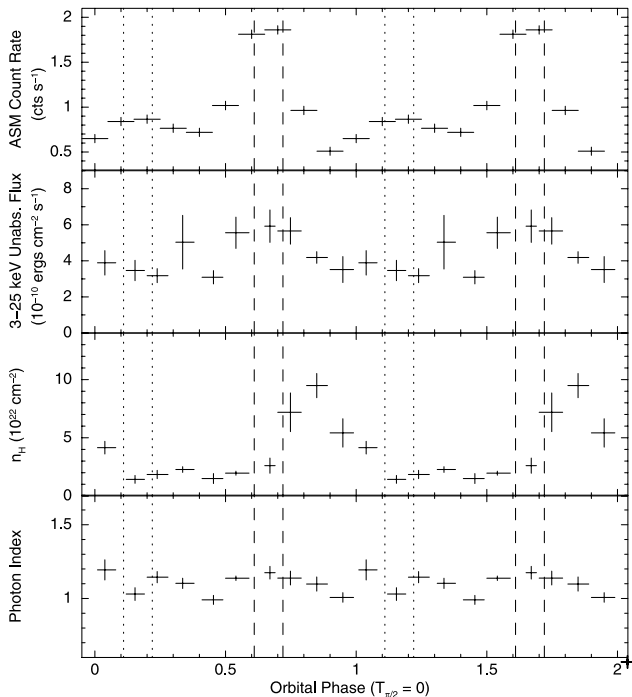

Figure 5. Variations of the spectral parameters through the binary orbit. For clarity, the data points are repeated for a cycle. From top to bottom, we show the *RXTE*/ASM folded orbital profile, the unabsorbed flux at 3–25 keV, the hydrogen column density and the photon index plotted over the orbital phase presented with 10 bins. All uncertainties are calculated at the 90 per cent confidence level. In all panels, the vertical dashed and dotted lines correspond to the times of the periastron and apastron passages, respectively, within 1σ.

not improve our fits, because this feature had lost its strength after the subtraction of the diffuse emission from the Galactic ridge.

The orbital variations of unabsorbed flux at 3–25 keV, the hydrogen column density (n_H) and the photon index are plotted in Fig. 5, which is an updated version of fig. 5 from İnam et al. (2009a). The variability of n_H over the binary orbit is evident in the third panel of Fig. 5. The base value of n_H is $\sim 2 \times 10^{22}$ cm^{-2}. It increases up

to a value of $\sim 10.5 \times 10^{22}$ cm^{-2} just after the periastron passage (indicated by the vertical dashed lines) and it remains at high values until the apastron, where it falls to its base value again. Nine of our individual n_H measurements exceed the previously reported maximal value ($\sim 9 \times 10^{22}$ cm^{-2} (In't Zand et al. 1997). A similar orbital dependence of n_H was also reported previously for the source (Roberts et al. 2001). We can see that there is no significant orbital variation of the photon index in the bottom panel of Fig. 5, where the mean value is ~ 1.1. Other parameters that are constant within the orbit are the high-energy cut-off and the exponential folding energy, with mean values 12.7 and 9.6 keV, respectively.

In some accretion-powered pulsars (e.g. Vela X-1; Haberl & White 1990), n_H is highly variable over the orbital phases and it can range up to $\sim 10^{23}$–10^{24} cm^{-2}. This variation can be used to probe the density distribution of the accreting matter. The observed increase in absorption at the periastron passage or eclipse ingress could be the result of a gas stream from the companion trailing behind the pulsar (Haberl, White & Kallman 1989). For 4U 1907+09, n_H increases to its maximum value after the periastron passage, which implies that the location of the absorbing material is the dense stellar wind of the companion star (Roberts et al. 2001). Leahy (2001) and Kostka & Leahy (2010) have modelled the absorption profile according to theoretical wind models. They have proposed that the most probable mechanism for 4U 1907+09 is accretion from a spherical wind with an equatorially enhanced dense spiral stream of gas around the companion star.

4.2 X-ray flux dependence of spectral parameters

In order to look for the X-ray flux dependence of the spectral parameters of the source, we have used the spectral parameters and X-ray flux values obtained from the 71 spectra presented in Section 4.1. We have sorted the observations according to the X-ray flux values, and the spectral parameters of the observations with similar X-ray flux values are averaged to obtain a spectral parameter set as a function of X-ray flux. It should be noted that the range of each flux value over which the spectral parameters are averaged is represented as the x-axis error bar of the data point in Fig. 6. We find that none of the spectral parameters, except for the power-law index, shows any correlation with the 3–25 keV unabsorbed X-ray flux; the power-law index is found to be correlated with the X-ray flux (see Fig. 6).
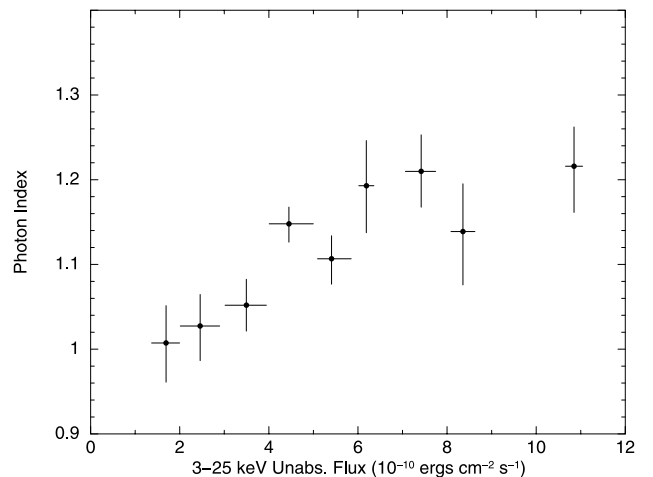

Figure 6. Variation of power-law index with X-ray flux from *RXTE*/PCA observations.

The correlation between the power-law index and the X-ray flux is an indication of spectral hardening with decreasing X-ray flux. A similar correlation has been seen in the accretion-powered pulsars V0332+53 (Klochkov et al. 2010), 4U 0115+63 (Klochkov et al. 2010), 4U 1626-67 (Jain, Paul & Dutta 2010) and Vela X-1 (Fürst et al. 2008). However, there are also some accretion-powered pulsars that exhibit spectral softening with decreasing X-ray flux: Her X-1 (Klochkov et al. 2010), Swift J1626.6-5156 (İçdem, İnam & Baykal 2011), XMMU J054134.7−682550 (İnam et al. 2009b), 2S 1417-62 (İnam et al. 2004) and SAX J2103.5+4545 (Baykal et al. 2007). Both the correlation and anticorrelation of the power-law index with X-ray flux might be considered as the result of the mass accretion rate variations and/or inhomogeneities in the companion's wind.

5 DIPPING STATES AND PULSE-TO-PULSE VARIABILITY

Because 4U 1907+09 is known to be a variable X-ray source, we have analysed the light curve of each *RXTE*/PCA observation to investigate the pulse-to-pulse variations. The source is known to have dipping episodes that show no pulsations (In't Zand et al. 1997), so we searched for irregularities of pulsations resulting from dipping ingress and egress. Although the short exposure time (∼2 ks) of the *RXTE* observations allow us to see at most about five successive pulses, we have been able to detect a variety of rapid pulse shape changes.

Fig. 7(a) gives an example of a pulsating and dipping light curve of 4U 1907+09. Generally, the pulse-to-pulse X-ray intensity decreases just before dipping ingress (see Fig. 7b) and it increases gradually after the dipping egress (see Fig. 7c). However, this is not the case for every dipping episode. The light curve in Fig. 7(d) is an extreme example, in which an X-ray flare follows a dipping episode, and after a smooth decrease for two pulses, the source again undergoes another dip. Although the pulse shape is conserved in these primary examples, we find that it can also be totally disrupted by the dip. For example, in Fig. 7(e) the pulse shape transforms to a single broad peak after a one pulse long dip and in Fig. 7(f) the attached wide peaks of the faint pulse are converted into detached sharp peaks after the dip. The beginning of the light curve in Fig. 7(f) is also an example of an unsuccessful dip, which can be observed occasionally (see also In't Zand et al. 1997). In Fig. 7(g), single peak pulses are observable before and after the 1.5 phase long dip. In Fig. 7(h), after two broad pulses, a dipping episode starts at phase 2.6 and continues until the end of the observation. A very rare condition is the total disappearance of only one peak of the pulse, as in Fig. 7(i); this example is the shortest dip that we observe (between phases 2.9 and 3.4). We observe that one pulse dips more commonly (e.g. the dip between phases 1.8 and 2.8 in Fig. 7j).

The dipping states observed in Vela X-1 (Kreykenbohm et al. 2008) have no identifiable transition phase in the spectra before or after the dip. However, in a recent study of GX 301-2, Göğüş, Kreykenbohm & Belloni (2011) have reported a spectral softening starting before the dip. The photon index, which reaches a maximum value during the peculiar dip of GX 301-2, resumes its normal value immediately after the dip. Fürst et al. (2011) have studied the dip spectra of GX 301-2 and they have found that although the pulses cease almost completely, n_H does not show any significant variation. For 4U 1907+09, a direct spectral study of the dips with *RXTE* is not possible because of the diffuse galactic emission background (i.e. the source is below the detection threshold and the dip spectra are similar to the Galactic ridge spectra). However, as seen from Fig. 8, the source can be observed in a dipping state in every orbital
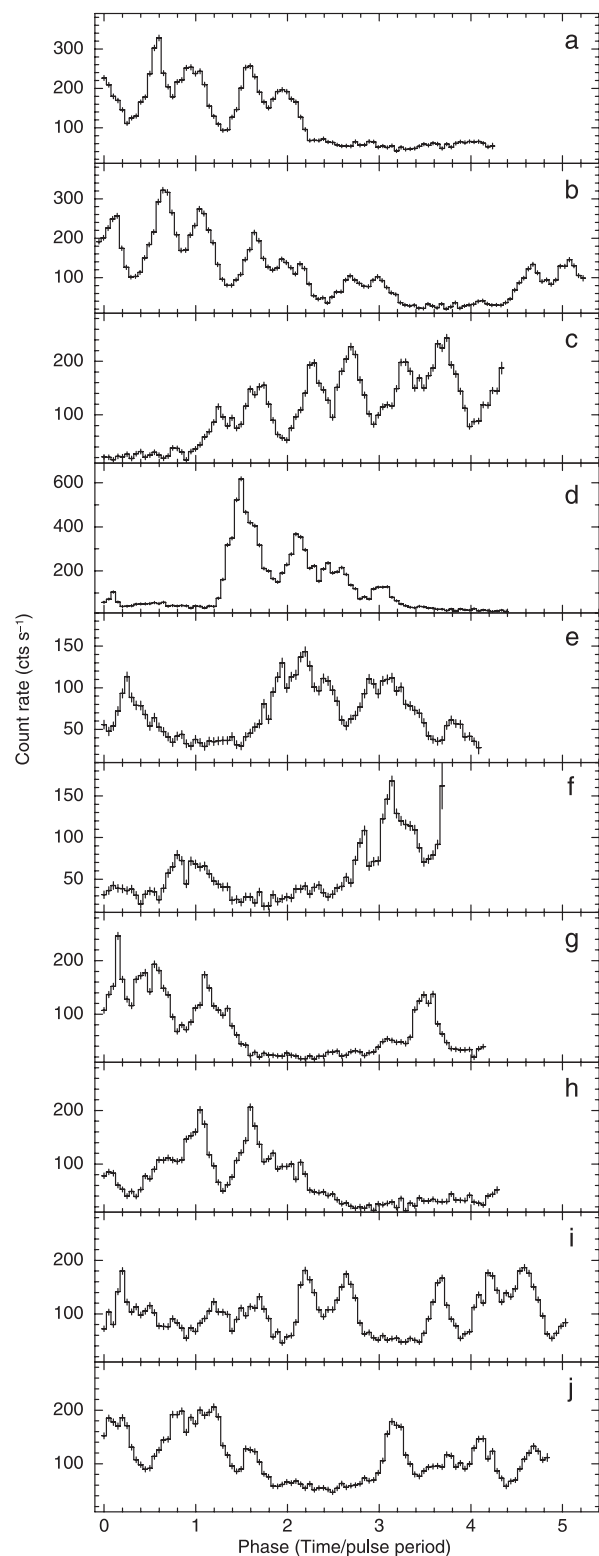

Figure 7. The sample set of 22-s binned light curves of different *RXTE*/PCA observations displays the variations of pulse shape from pulse-to-pulse and the irregularities as a result of dipping activity. Time values are converted to phases (or time/pulse period) for arbitrary observation epochs. Explanations for each panel are given in Section 5. The observation IDs of the panels from top to bottom are (a) 94036-01-19-00, (b) 96366-02-01-00, (c) 94036-01-05-00, (d) 94036-01-23-00, (e) 94036-01-13-00, (f) 93036-01-20-00, (g) 94036-01-03-00, (h) 93036-01-34-00, (i) 93036-01-38-00 and (j) 95350-01-06-00.
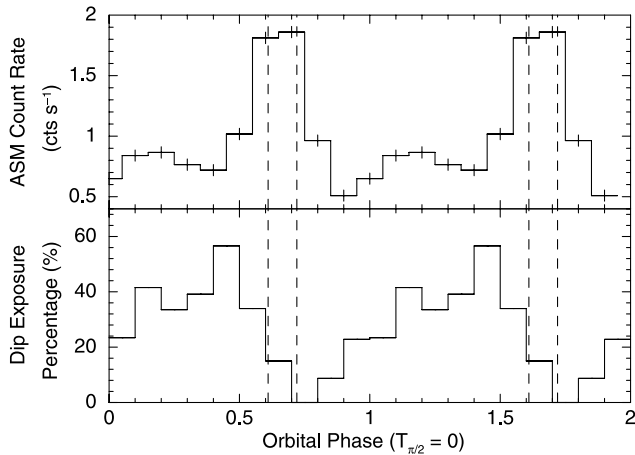
Figure 8. ASM light curve folded at the orbital period (top panel) and the percentage of dip exposure times to the total exposure through the binary orbit (bottom panel). For clarity, the data points are repeated for a cycle. The vertical dashed lines correspond to the time of periastron passage within 1σ. It is evident that the probability of observing a dipping state is lower during the periastron passage and afterwards (between orbital phases 0.6 and 0.9).

phase apart from the phases between 0.7 and 0.8. Comparing this result with the spectral results of non-dipping observations (see Fig. 5), the absence of dips matches with the orbital phases when n_H reaches its maximum value just after the periastron passage (see the bottom panel of Fig. 8). Moreover, the possibility of dipping is less in the orbital phases from 0.8 to 1.1 when compared to phases from 0.1 to 0.6, which does not correlate with the n_H values. The source frequently undergoes dipping states during the times with minimum n_H, and the possibility of this peaks between the phases 0.4 and 0.5. It is important to note that this is not a strong conclusion, because we are not able to directly measure the spectral parameters of the dips.

Recently, it has been suggested that the strongly structured wind of the optical companion is the reason for the dips in the HMXB light curves. The clumpy wind of the companion, which is highly inhomogeneous, creates regions of different densities. Recent models have shown that the density of the wind material can change by up to several orders of magnitude (Runacres & Owocki 2005). Therefore, a sudden decrease of X-ray luminosity is caused by the decrease in the mass accretion rate. As the accretion rate decreases, the Alfvén radius increases and accretion stops when the source enters the propeller regime. Hence, the disappearance of pulsations can be explained by the passage of the pulsar through low-density regions of the wind. The limit to the luminosity that turns on the propeller mechanism can be derived from the condition where the magnetospheric radius is equal to the corotation radius (Illarionov & Sunyaev 1975), which is 6×10^{31} erg s^{-1} for 4U 1907+09. Therefore, the dipping states are candidate episodes for the propeller regime because the count rates are below the detection threshold. A similar propeller transition is suggested as the cause of the dips observed in the accretion-powered pulsars GX 1+4 and GRO J1744-28 (Cui 1997). The dipping episodes of 4U 1907+09 are known to have irregular time coverage, with varying durations. We investigate the distribution of dipping states through the orbital phase. About 46 of the 98 observations include dipping states. The percentage of exposure time spent in dipping is ∼28 per cent of the total exposure. In order to obtain the orbital distribution of dipping states, we calculate the percentage of the dip exposure to total expo-

sure, corresponding to each orbital phase with 0.1 phase resolution. In Fig. 8, we plot the variation of the dip exposure percentage with the orbital phase, together with the folded All-Sky Monitor (ASM) light curve at the orbital period. It is clearly seen that the occurrence of dips sharply decreases during the periastron passage and after the passage. Around the periastron passage, the ASM count rate and, therefore, the X-ray flux increase, whereas the number of dip states decreases. It should be kept in our mind that a transient quasi-periodic oscillation was found during one of the flares, which suggests the formation of a transient disc (In't Zand et al. 1997). This implies that there are fewer occurrences of dip states at the periastron passage and afterwards, because disc accretion is the dominant mechanism. After the apastron (phases 0.1–0.5), the number of dip states increases because of the clumpy nature of accretion, and the occurrence of transient propeller regime episodes increases, which naturally explains the variable nature of the spin-down. The combination of disc and wind accretion at different orbital phases might lead to the random walk nature of the pulse frequency time series.

6 SUMMARY

In this paper, we present an analysis of the accretion powered pulsar 4U 1907+09 using observations from *INTEGRAL* IBIS–ISGRI (between 2005 October and 2007 November) and *RXTE*/PCA (between 2007 June and 2011 March).

Using the *INTEGRAL* and *RXTE* observations, we report on new pulse period measurements, and we obtain an updated version of the pulse period history of İnam et al. (2009a), as shown in Fig. 3. Using these measurements, we construct the power spectrum density of the pulse frequencies (see Fig. 4). We find that the fluctuations in the pulse frequency derivatives are white noise and that the pulse frequency fluctuations are consistent with the random walk model. The noise strength is found to be 1.27×10^{-21} Hz s^{-2}. We infer that for short time-scales, there might be transient disc formation around the neutron star, which causes random walk in the pulse frequency, while in the long term the spin-down rate is steady.

From the X-ray spectral analysis of the *RXTE*/PCA observations, we find that only the hydrogen column density (n_H) is significantly variable over the binary orbit; it tends to increase just after the periastron passage (see Fig. 5). This might indicate that the location of the absorbing material is the dense stellar wind of the companion star. We also study the flux dependence of the spectral parameters and we find that power-law index shows a correlation with the 3–25 keV unabsorbed X-ray flux. This indicates spectral hardening with a decreasing X-ray flux (see Fig. 6). This spectral variation might be related to variations in the mass accretion rate and/or inhomogeneities in the companion's wind.

We also look for irregularities of pulsations near dipping ingress and egress (see Fig. 7). We propose that the disappearance of pulsations can be explained by the passage of the pulsar through the low-density regions of the clumpy wind. This might lead to a temporary propeller state being turned on, so that the X-ray luminosity decreases below the detection threshold. We are able to analyse the orbital dependence for the occurrences of the dip state (see Fig. 8). We find that the source more likely undergoes dipping states after the apastron until the periastron, where transitions to a temporary propeller state might occur because of accretion from the clumpy wind.

ACKNOWLEDGMENTS

REFERENCES

Baykal A., İnam S. Ç., Alpar M. A., In't Zand J., Strohmayer T., 2001, MNRAS, 327, 1269
Baykal A., İnam S. Ç., Beklen E., 2006, MNRAS, 369, 1760
Baykal A., İnam S. Ç., Stark M. J., Heffner C. M., Erkoca A. E., Swank J. H., 2007, MNRAS, 374, 1108
Bildsten L. et al., 1997, ApJS, 113, 367
Chitnis V. R., Rao A. R., Agrawal P. C., Manchanda R. K., 1993, A&A, 268, 609
Coburn W., Heindl W. A., Rothschild R. E., Gruber D. E., Kreykenbohm I., Wilms J., Kretschmar P., Staubert R., 2002, ApJ, 580, 394
Cook M. C., Page C. G., 1987, MNRAS, 225, 381
Corbet R. H. D., 1984, A&A, 141, 91
Cordes J. M., 1980, ApJ, 237, 216
Cox N. L. J., Kaper L., Mokiem M. R., 2005, A&A, 436, 661
Cui W., 1997, ApJ, 482, L163
Cusumano G., di Salvo T., Burderi L., Orlandini M., Piraino S., Robba N., Santangelo A., 1998, A&A, 338, L79
Deeter J. E., 1981, PhD thesis, Washington Univ. Seattle
Deeter J. E., 1984, ApJ, 281, 482
Deeter J. E., Boynton P. E., 1985, in Hayakawa S., Nagase F., eds, Proc. Inuyama Workshop: Timing Studies of X-Ray Sources. Nagoya Univ., Nagoya, p. 29
Deeter J. E., Boynton P. E., Lamb F. K., Zylstra G., 1989, ApJ, 336, 376
Fritz S., Kreykenbohm I., Wilms J., Staubert R., Bayazit F., Pottschmidt K., Rodriguez J., Santangelo A., 2006, A&A, 458, 885
Fürst F., Kreykenbohm I., Wilms J., Kretschmar P., Klochkov D., Santangelo A., Staubert R., 2008, in Proc. 7th *INTEGRAL* Workshop: An *INTEGRAL* View of Compact Objects, PoS Integral08:119 (arXiv:0903.0832)
Fürst F., et al., 2011, A&A, 535, 9
Giacconi R., Kellogg E., Gorenstein P., Gursky H., Tananbaum H., 1971, ApJ, 165, L27
Göğüş E., Kreykenbohm I., Belloni T. M., 2011, A&A, 525, L6
Haberl F., White N. E., 1990, ApJ, 361, 225
Haberl F., White N. E., Kallman T. R., 1989, ApJ, 343, 409
İçdem B., İnam S. Ç., Baykal A., 2011, MNRAS, 415, 1523
Illarionov A. F., Sunyaev R. A., 1975, A&A, 39, 185
İnam S. Ç., Baykal A., Scott D. M., Finger M., Swank J., 2004, MNRAS, 349, 173
İnam S. Ç., Şahiner Ş., Baykal A., 2009a, MNRAS, 395, 1015
İnam S. Ç., Townsend L. J., McBride V. A., Baykal A., Coe M. J., Corbet R. H. D., 2009b, MNRAS, 395, 1662
In't Zand J. J. M., Strohmayer T. E., Baykal A., 1997, ApJ, 479, L47
In't Zand J. J. M., Baykal A., Strohmayer T. E., 1998, ApJ, 496, 386
Iye M., 1986, PASJ, 38, 463
Jahoda K., Swank J. H., Giles A. B., Stark M. J., Strohmayer T., Zhang W., Morgan E. H., 1996, Proc. SPIE, 2808, 59
Jain C., Paul B., Dutta A., 2010, MNRAS, 403, 920
Klochkov D., Santangelo A., Staubert R., Rothschild R. E., 2010, in Proc. 8th *INTEGRAL* Workshop, The Restless Gamma-Ray Universe, PoS(INTEGRAL 2010)061 (arXiv:1105.3547)
Kostka M., Leahy D. A., 2010, MNRAS, 407, 1182
Kreykenbohm I. et al., 2008, A&A, 492, 511
Leahy D. A., 2001, in Proc. 27th International Cosmic Ray Conference. Copernicus Gesellschaft, Hamburg, p. 2528
Leahy D. A., Darbro W., Elsner R. F., Weisskopf M. C., Kahn S., Sutherland P. G., Grindlay J. E., 1983, ApJ, 266, 160
Lebrun F. et al., 2003, A&A, 411, L141
Makishima K., Kawai N., Koyama K., Shibazaki N., 1984, PASJ, 36, 679
Makishima K. et al., 1990, PASJ, 42, 295
Makishima K., Mihara T., Nagase F., Tanaka Y., 1999, ApJ, 525, 978
Marshall N., Ricketts M. J., 1980, MNRAS, 193, p7
Mihara T., 1995, PhD thesis, RIKEN, Tokyo
Mihara T., Makishima K., Ohashi T., Sakao T., Tashiro M., 1990, Nat, 346, 250
Mukerjee K., Agrawal P. C., Paul B., Rao A. R., Yadav J. S., Seetha S., Kasturirangan K., 2001, ApJ, 548, 368
Nespoli E., Fabregat J., Mennickent R. E., 2008, A&A, 486, 911
Rivers E et al., 2010, ApJ, 709, 179
Roberts M. S. E., Michelson P. F., Leahy D. A., Hall T. A., Finley J. P., Cominsky L. R., Srinivasan R., 2001, ApJ, 555, 967
Runacres M. C., Owocki S. P., 2005, A&A, 429, 323
Şahiner Ş., İnam S. Ç., Baykal A., 2011, in Göğüş E., Belloni T., Ertan Ü., eds, Proc. AIP Conf. Vol. 1379, Astrophysics of Neutron Stars 2010: A Conference in Honor of M. Ali Alpar. American Institute of Physics, New York, p. 214
Schwartz D. A., Griffiths R. E., Bowyer S., Thorstensen J. R., Charles P. A., 1980, AJ, 85, 549
Ubertini P. et al., 2003, A&A, 411, L131
Wilms J., Nowak M. A., Dove J. B., Fender R. P., Di Matteo T., 1999, ApJ, 522, 460

This paper has been typeset from a TEX/LATEX file prepared by the author.